Machine learning enabled electrical impedance tomography

Frederik Brooke Barnes

Department of Physics and Astronomy

The University of Manchester

MPhys Project

January 2021

Contents

1 Introduction

Electrical impedance tomography (EIT) is an electrical imaging technique used to map the electrical properties of a two or three-dimensional object through electrical measurements taken on the outside of the sample. EIT has applications in medical imaging [1], solid state physics [2], and chemical engineering [3]. Advantages of EIT include that it is non-invasive, low cost, and scalable [4]. However, a key disadvantage is its low spatial resolution [4][5].

Typically a four-electrode method is used to measure the impedance between contacts placed around the boundary of a sample. Using these measurements, an algorithm can be used to determine the distribution of electrical permittivity within the sample. As the accuracy and resolution of the distribution can be improved by taking impedance measurements from a greater number of electrode positions, it is can be desirable to increase the number of contacts [6]. However, this results in a greater number of measurements to be taken and therefore comes at a cost of increasing the time required to make a scan and calculate a solution. Therefore, it is desirable to know which electrode positions are likely to provide more information than others. As this is not generally known a priori, it is proposed that an electrode selection algorithm (ESA) based on machine learning can be used in real-time to suggest the optimal electrode positions to be used for measurement while the scan is in progress. This reduces the number of measurements required to achieve an acceptable resolution given a certain number of contacts. Therefore, a greater number of contacts can be used, providing greater resolution, without the cost in time required to take more measurements.

2 Objectives

The aim of this project was to evaluate whether using such an ESA provides a useful speed-up when scanning samples of interest in solid state physics. In particular, this was done with the intention of performing EIT on graphene and graphene-based devices. Although EIT of graphene was not carried out, EIT scans of two different resistor networks, which acted as a simplistic model of a two-dimensional material with spatially varied resistivity, were carried out.

Much of the work in developing an ESA and optimising the existing EIT algorithms used in this project was done by previous MPhys students at the University of Manchester. However, this is the first time it has been attempted to use the ESA in a practical context. Therefore, one of the main challenges of this project was integrating previously developed software and interfacing it efficiently with the appropriate instrumentation. This project was a collaborative effort with my lab partner, Adam Coxson. In general, we worked on each aspect

of the project together. However, I focused more on the software required to interface with the hardware and Adam Coxson focused more on adapting the ESA. Despite the experimental nature of this project, all of our work was done remotely due to coronavirus restrictions. Therefore, thanks must be given to the members of Prof Mishchenko's group at the University of Manchester whose help in the lab made this project possible.

The result was that we were able to demonstrate a system suitable for machine learning enabled EIT. However, more work must be done to show that the use of an ESA does provide a useful speed-up, paving the way for future high-resolution EIT systems for use in solid state physics.

3 Theory

3.1 Electrical impedance tomography

The principle of EIT is to take electrical measurements on the boundary of an object in order to obtain information about the admittivity of the whole sample. Each measurement requires two pairs of electrodes. A current is driven between one pair and the voltage between the other pair is measured. So, how can we gain information about the interior of the sample given only information about the boundary?

In order to tackle this problem, we can consider Maxwell's laws. Doing so, we obtain Poisson's equation,

$$\nabla \cdot \sigma \nabla V = 0, \tag{1}$$

where V is the electric potential and σ is the admittivity. The admittivity is the reciprocal of the impedance of the material, and is in general complex. For low frequencies, the complex part of the admittivity can be neglected leaving the real part which is the conductance of the material [7]. According to the uniqueness theorem, given σ and the boundary values of V, there is a single solution to Equation 1. For simple cases this can be done analytically. However, for more complex cases as used in EIT, a solution must be found numerically. The process of finding such a solution is known as the forward problem. In contrast, the process of finding σ given a finite set of boundary measurements is known as the inverse problem and, in general, does not have a unique solution; therefore, the inverse problem is ill-posed. Algorithms used to solve the inverse problem often rely on a solution to the forward problem. Hence, the forward problem will be discussed in the following section.

3.1.1 Forward problem

The forward problem can be solved using a finite element method (FEM). Firstly, we consider the surface of interest, Ω, and its boundary, $\partial\Omega$. Ω is discretised by creating a mesh of N triangles which form the elements of the model. The vertices formed by the mesh are known as nodes. Electrode contact points correspond to labelled nodes on the boundary of the mesh. A single contact may be modelled as a single node or by multiple nodes to account for the finite size of the contacts. An example used in this project is shown in Figure 1. Further considerations of the contact, such as contact potential and impedance, may be modelled using a complete electrode model [8]. However, this was not done as part of this project.

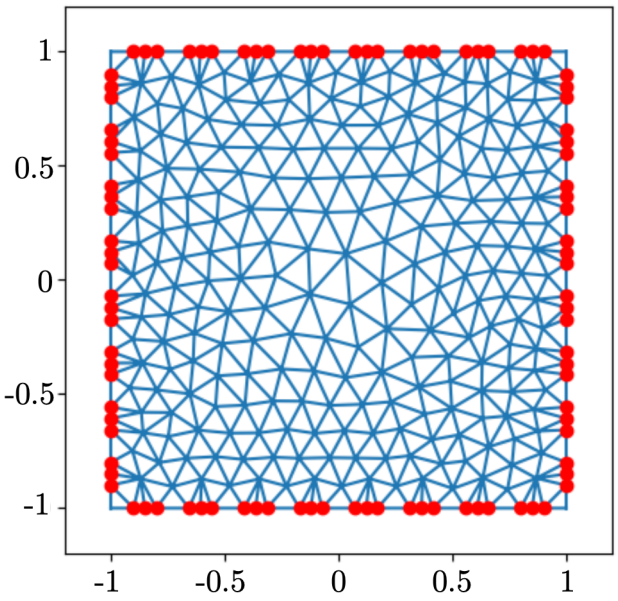

Figure 1: Example plot of the meshing used in the forward model. Axes are in units of arbitrary length. The square was discretised into triangular elements. Red dots show 96 nodes corresponding 3 nodes per 32 electrode contact. The mesh was created in Python using PyEIT [9].

The electrical potential within an element can be written as a sum of interpolation functions:

$$V(x,y) = \sum_i V_i f_i(x,y). \tag{2}$$

Here, $i = 1, 2, 3$ for each of the nodes in each triangular element, V_i is the electric potential on each element, and $f_i(x,y)$ is a dimensionless function of position which equals 1 at node i and 0 at the other two nodes. There is a choice of the

form of f_i, such as a polynomial. A matrix, $\mathbf{y}$, for each triangle is calculated as

$$y_{ij} = \sigma \iint_A \left(\frac{\partial f_i}{\partial x} \frac{\partial f_j}{\partial x} + \frac{\partial f_i}{\partial y} \frac{\partial f_j}{\partial y} \right) dA, \tag{3}$$

where A is the surface of the triangle. To represent all of the triangles, an $N \times N$ matrix, $\mathbf{Y}$, is assembled from each $\mathbf{y}$ such that the electric field is the same at the nodes where triangles are connected. This matrix can then be used to form the linear system of equations

$$\mathbf{Y}\boldsymbol{v} = \boldsymbol{c} \tag{4}$$

where $\boldsymbol{v}$ is a vector of the electric field at each node, and $\boldsymbol{c}$ is a vector of the current at each node. These vectors represent the Dirichilet and Neumann boundary conditions, respectively. Finally, Equation 4 can then be solved directly or iteratively [10]. This was done using a forward solver implemented in PyEIT and optimised for parallel processing as described in [11].

Once the forward model has been established, the Jacobian, $\mathbf{J}$, may be calculated. Its elements are defined as

$$J_{ijk} = \frac{\partial V_{ij}}{\partial \sigma_k} = \int_{\Omega_k} \nabla V_i \cdot \nabla V_j \; ds, \tag{5}$$

where V_{ij} is the voltage between electrodes i and j, σ_k is the conductivity of element k in the forward model, and the integral is over the kth element's surface, Ω_k. The Jacobian is useful in the inverse problem and in the electrode selection algorithms discussed in the following sections.

3.1.2 Inverse problem

The inverse problem is a nonlinear problem [12]. However, linearised approximations have been shown to be useful in EIT reconstruction algorithms; the inverse problem in this project was solved using the Graz consensus reconstruction algorithm for EIT (GREIT) [13]. GREIT is a difference EIT algorithm which reconstructs a vector of conductivity change, $\mathbf{x} = \boldsymbol{\sigma} - \boldsymbol{\sigma_r}$, where $\boldsymbol{\sigma_r}$ is a known reference conductivity and $\boldsymbol{\sigma}$ is the conductivity of the sample being measured. The linear approximation assumes that a set of EIT voltage measurements, $\mathbf{v}$, can be used to calculate $\mathbf{x}$ using a reconstruction matrix $\mathbf{R}$ through the relationship

$$\mathbf{x} = \mathbf{R}\mathbf{y}. \tag{6}$$

GREIT acknowledges that the resolution of EIT is limited and therefore small features in $\mathbf{x}$ will be blurred. So, rather than attempting to reconstruct $\mathbf{x}$ exactly, GREIT attempts to construct $\tilde{\mathbf{x}}$

$$\tilde{\mathbf{x}} = \mathbf{D}\mathbf{x}, \tag{7}$$

where $\mathbf{D}$ is a matrix which represents a blurring operation on $\mathbf{x}$. Each element in $\mathbf{x}$ will influence a number of elements in $\tilde{\mathbf{x}}$ depending on the choice of blurring used, the degree to which is determined by a weighting, $\mathbf{w}$. GREIT is designed to be trained over a large number of training samples which may be simulated or from previous experiment. Therefore, $\mathbf{R}$ is calculated as the matrix which minimises the error, ϵ^2:

$$\epsilon^2 = E_w[||\tilde{\mathbf{x}} - \mathbf{R}\mathbf{y}||^2], \tag{8}$$

where

$$E_w[x] = \frac{1}{N}\sum_{i=1}^{N} w_i x_i, \tag{9}$$

is the weighted mean over N training samples. To find the minimum of Equation 8, we differentiate and set to zero such that

$$\frac{\partial}{\partial \mathbf{R}}\epsilon^2 = E_w\left[\frac{\partial}{\partial \mathbf{R}}||\tilde{\mathbf{x}} - \mathbf{R}\mathbf{y}||^2\right] = -2E_w[(\tilde{\mathbf{x}} - \mathbf{R}\mathbf{y})\mathbf{y}^T] = 0. \tag{10}$$

Therefore, $\mathbf{R}$ is given by

$$\mathbf{R} = E_w[\tilde{\mathbf{x}}\mathbf{y}^T](E_w[\mathbf{y}\mathbf{y}^T])^{-1}. \tag{11}$$

In order to calculate $\mathbf{R}$, the distribution method was used. Rather than using real or simulated training data, the distribution method allows direct calculation of $\mathbf{R}$ by making assumptions about the statistics of an appropriate set of training data and the measurement noise. The argument that follows can be found in greater detail in [14]. Firstly, we assume that $\mathbf{x}$ for the training samples is distributed normally about a mean of zero and a covariance of $\boldsymbol{\Sigma_x}$. Secondly, we assume that there is a measurement noise $\mathbf{n}$ which is also distributed normally about zero and with a covariance of $\boldsymbol{\Sigma_n}$. Furthermore we write that

$$\mathbf{y} = \mathbf{J}\mathbf{x} + \mathbf{n}, \tag{12}$$

where $\mathbf{J}$ is the Jacobian of the FEM model described in Section 3.1.1. Therefore,

$$E_w[\mathbf{y}\mathbf{y}^T] = \mathbf{J}E_w[\mathbf{x}\mathbf{x}^\mathbf{T}]\mathbf{J}^\mathbf{T} + E_w[\mathbf{n}\mathbf{n}^\mathbf{T}] = \mathbf{J}\boldsymbol{\Sigma}^*_\mathbf{x}\mathbf{J}^\mathbf{T} + \boldsymbol{\Sigma}_\mathbf{n}, \tag{13}$$

and

$$E_w[\tilde{\mathbf{x}}\mathbf{y}^T] = \mathbf{D}E_w[\mathbf{x}\mathbf{x}^\mathbf{T}]\mathbf{J}^\mathbf{T} = \mathbf{D}\boldsymbol{\Sigma}^*_\mathbf{x}\mathbf{J}^\mathbf{T}, \tag{14}$$

where $\boldsymbol{\Sigma}^*_{\boldsymbol{x}}$ is the covariance weighted by $\mathbf{w}$. $\boldsymbol{\Sigma_n}$ remains unchanged as we assume the noise is independent of location. Finally, using Equation 11, we find the reconstruction matrix is given by

$$\mathbf{R} = \mathbf{D}\boldsymbol{\Sigma}^*_\mathbf{x}\mathbf{J}^\mathbf{T}(\mathbf{J}\boldsymbol{\Sigma}^*_\mathbf{x}\mathbf{J}^\mathbf{T} + \lambda\boldsymbol{\Sigma}_\mathbf{n})^{-1}, \tag{15}$$

which is in the form of the solution to Tikhonov regularisation, with the regularisation parameter λ controlling the noise performance of the reconstruction [15]. In this project, the blurring matrix, $\mathbf{D}$, was based on a uniform weighting matrix with blurring using a sigmoid function; this was done using GREIT algorithm as implemented in PyEIT [9].

3.2 Electrode selection algorithm

3.2.1 Traditional algorithms

Each EIT measurement can be labelled by the position of the pair of electrodes used to drive a current and the pair of electrodes used to measure the resulting voltage. Typically, there are fixed contacts made to the sample and measurement positions are changed via electrical or mechanical switching. As the minimum feature size distinguishable by EIT can be approximated by the distance between regularly spaced electrodes, it is desirable to increase the number and therefore density of electrodes used. The number of possible measurements, n_{total}, which may be made using n_{el} electrodes in isotropic materials is given by

$$n_{total} = P(n_{el}, 4) = \frac{1}{4}\frac{n_{el}!}{(n_{el}-4)!}. \tag{16}$$

Here, we divide the number of permutations by 4. This is due to the fact that for isotropic materials (where σ is described by a scalar rather than a rank-2 tensor), changing the polarity of the contacts does not affect the measurements. Due to the factorial nature of Equation 16, we see that the n_{total} rises rapidly with increasing n_{el}. This results in a rapidly increasing length of time required to take each scan and an increase in the computational memory and processing resources required. Typically, the number of measurements used per scan is limited by using an electrode selection algorithm (ESA).

A common ESA is known as the adjacent-adjacent method, in which adjacently positioned pairs of electrodes are used for the current and adjacently positioned pairs are used for the voltage [2]. This results in $n_{adj\text{-}adj}$ measurements per scan, given by

$$n_{adj\text{-}adj} = n_{el}(n_{el} - 3). \tag{17}$$

We also found that similar methods such as adjacent-opposite, opposite-adjacent, and opposite-opposite also scale quadratically with n_{el}. This style of ESA is commonly used in EIT, with GREIT being specified for use with the adjacent-adjacent method [13]. However, since the development of GREIT, it has been shown that the adjacent-adjacent method is in fact one of the poorest performing ESAs [16]. In contrast, using an adaptive ESA, which suggests new measurement positions as the scan progresses, has been shown to provide increased performance, as discussed in the following section.

3.2.2 Adaptive algorithm

A detailed explanation of a novel adaptive ESA, developed by Mihov and Avramov, can be found in [11]. This adaptive ESA is based on two assumptions:

1. Each new voltage measurement provides additional information, although total error could increase.

2. The probability for the GREIT algorithm to miss a deviation in conductivity is greater close to an already located deviation, where the gradient of the conductivity is larger.

The main objective of the algorithm is to locate the zones of interest in the sample. The algorithm achieves this by combining two approaches:

1. Measure close to the boundary of found deviations, according to Assumption 2.

2. Measure the zones affected least by the previous measurements.

To quantify the degree to which Approach 1 applies to each element in the model of the sample, a deviation map, $\mathbf{D}$, is calculated as

$$\mathbf{D} = \mathbf{G} \circ \mathbf{L}^{\circ q}, \tag{18}$$

where $\mathbf{G}$ is a map of the gradient of σ, $\mathbf{L}$ is the logarithm of σ, and q is a parameter to be found through optimisation. $\circ$ represents an element-wise operation. To quantify the degree to which Approach 2 applies to each element in the model of the sample, an influence map, $\mathbf{S}$, is calculated as

$$\mathbf{S} = \sum_k |\Delta\sigma_k|, \tag{19}$$

where $\Delta\sigma_k$ is the difference in conductivity between the conductivity reconstructed from the voltage measurements made so far and the conductivity reconstructed when the kth measurement is perturbed by an amount p. To combine the two approaches, a total map, $\mathbf{T}$ is calculated as

$$\mathbf{T} = \mathbf{D} \circ \mathbf{S}^{\circ r}, \tag{20}$$

where t is a parameter to be optimised.

To select a pair of current electrodes, we assume that the conductivity of the elements along a direct path between any two electrodes has the most influence on the total resistance; of course, this is a simplification as current does not simply pass as a ray. Subsequently, we sum the elements of $\mathbf{T}$ which lie on this path for each current pair. The current pair with the greatest sum is then chosen.

To select a pair of voltage electrodes, we consider the Jacobian, $\mathbf{J}$, as defined in Equation 5. The Jacobian is also known as the sensitivity matrix and is a measure of how the voltage between two electrodes is affected by a change in

conductivity of an element in the forward model. We then consider the elements, k, which lie within zones of interest according to our assumptions, which is given by $T_k > t \max(\mathbf{T})$, where t is a parameter to be optimised between 0 and 1. Subsequently, we sum the elements of $\mathbf{J}$ over the elements of interest for each voltage pair. The voltage pair with the greatest sum is then chosen.

The parameters p, q, r, and t are all real numbers which need to be optimised by training the algorithm with a set of training samples relevant to the target samples of interest. In this project, we used the parameters found in [11]:

$$\begin{aligned} p &= 0.5, \\ q &= 10, \\ r &= -10, \\ t &= 0.97 \end{aligned}$$

These parameters were found using Bayesian optimisation and a training set of 1000 randomised square samples. However, it should be noted that the values of the parameters q and r were limited by the bounds (± 10) applied to the optimisation process. Due to q lying on the upper limit and r lying on the lower limit, it suggests that the optimisation process favoured Approach 1. Despite these limitations, it was shown that the adaptive ESA performed better than both the traditional opposite-adjacent and adjacent-adjacent methods when using simulated samples [11].

4 Experimental approach

4.1 Equipment and Software

A schematic of the experimental setup is shown in Figure 2.

A Stanford Research Sytstems SR860 lock-in amplifier was used to both measure electrode voltages and provide the driving current. The lock-in amplifier was used in differential mode, allowing the measurement of voltages between inputs V_+ and V_-. The driving current was provided by using the lock-in amplifier's built-in sine-wave reference signal generator in series with a shunt resistor of $100\,\mathrm{k\Omega}$ (nominal) to provide an alternating current source of $10\,\mu\mathrm{A}$. This was output in differential mode between outputs I_+ and I_-.

In order to switch the outputs/inputs of the lock-in amplifier between different electrode pairs, a Cytech VX/256 switchboard was used allowing the four lock-in connections to be switched between up to 64 electrodes, although only 32 electrodes were used during this project. Connections between the lock-in amplifier, switchboard, and sample were made using coaxial cable with BNC connections.

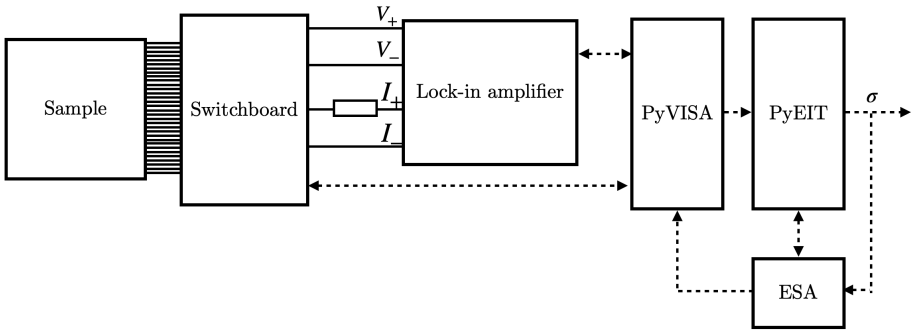

Figure 2: Schematic of the experimental setup and computational process used in the project. Solid lines show physical electrical connections. Dotted arrows show the transfer of digital information between software modules. V_+ and V_- are the electrode voltage measurements made by the lock-in amplifier. I_+ and I_- are the outputs of the lock-in amplifier with a shunt resistor at I_+. σ is the reconstructed conductivity map.

Both the lock-in amplifier and switchboard were connected to a PC to allow automated measurement; this was done by Ethernet and GPIB, respectively. The instrumentation was interfaced with the PC using the Python package PyVISA [17]. The PC had an NVidia CUDA-compatible graphics card, allowing parallelisation of array-based calculations using CuPy [18]. PyEIT was used to implement the GREIT reconstruction algorithm [9][13].

4.2 Samples

Two samples were used in the course of the project. Both were networks of resistors arranged in a square grid, as shown in Figure 3. The resistances were chosen to reflect the typical sheet resistances of CVD graphene which is on the order of 100s of $\Omega/\square$ [19]. As the sheet resistance is not dependent on the scale of the sample, this was appropriate [20].

4.3 Methodology

4.3.1 Measurement protocol

As discussed in Section 3.2.1, the number of measurements per scan grows rapidly with the number of electrodes used. Furthermore, performing scans in rapid succession is also useful for dynamic EIT. Therefore, a desirable quality of an EIT system is the ability to take accurate measurements at a rapid

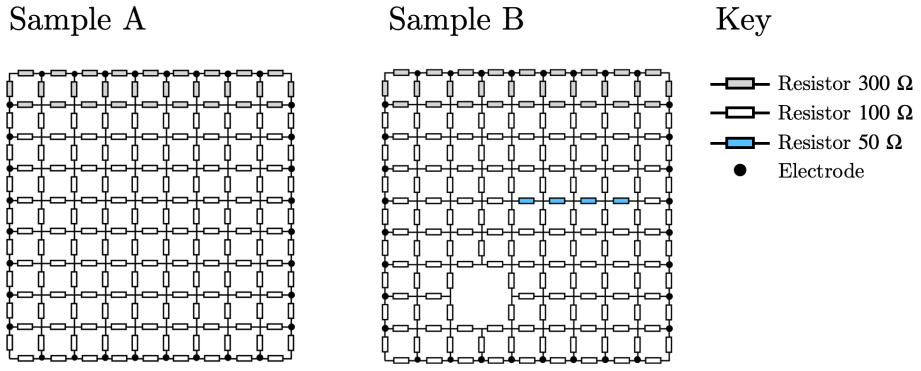

Figure 3: Diagram of the resistor grid samples used in the project. Sample A is made from 81 SMD resistors soldered together. Sample B is made by removing four resistors from one region of Sample A and soldering them in parallel to another four to produce 50 Ω. 32 electrodes are shown as dots which were connected to the switchboard by BNC coaxial cables.

rate. When using a lock-in amplifier, the minimum time required to take a measurement is often determined by the time constant used. The time constant refers to the time constant of the low-pass resistor-capacitor (RC) filters used in older lock-in amplifiers and is given by

$$\tau = \frac{1}{2\pi f_c} = RC, \tag{21}$$

where f_c is the cut-off frequency. Usually it takes several time constants for a measurement to settle. Therefore, the driving frequency is related to the maximum sampling rate. In order to determine an appropriate driving frequency to use in this experiment, a frequency response graph for a four-contact voltage measurement was carried out, as shown in Figure 4.

In modern lock-in amplifiers, such as the one used in this project, filtering is done with advanced digital filters. However, an effective time constant must still be chosen and this is dependant on the driving frequency. In practice, it is necessary to determine experimentally the time required to take each measurement for a given frequency. This was especially true for the EIT system being considered, as it was necessary to also take into account the delay between the time when the code instructing the switchboard to change its state is executed and the time when the operation is fully completed. Therefore, using an 8 kHz signal, it was found that the shortest delay time required to wait before taking a reading was approximately 20 ms and with a time constant of 1 ms. This was determined by plotting a two-contact resistance measurement as a function of the delay time, as shown in Figure 5, and finding the time at which the resistance becomes constant

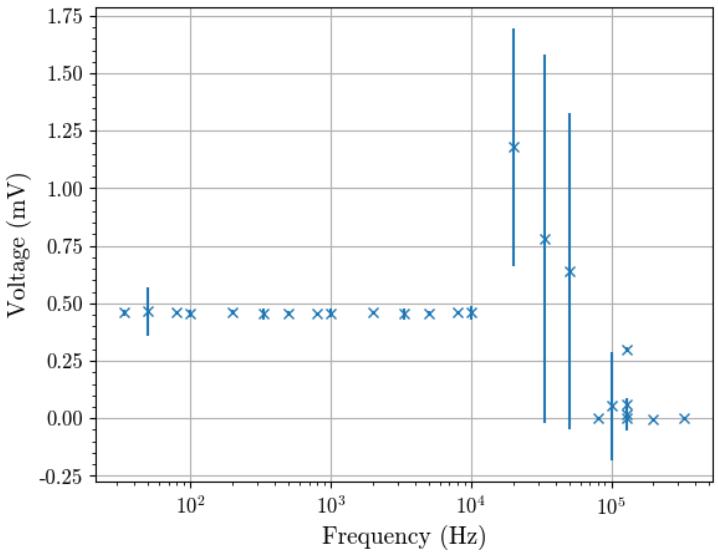

Figure 4: Plot of a four-contact voltage measurement as a function of driving signal frequency. For each frequency, the relationship between the period of the driving signal and time constant was kept constant (rounded to the nearest time constant available on the lock-in amplifier). Stable measurement was determined to be possible up to 8 kHz.

and the error becomes small. Here, we define the two-contact resistance as

$$R = \frac{V_+ - V_-}{I}, \tag{22}$$

where $V_+ - V_-$ is the peak-to-peak voltage measured by the lock-in amplifier, I is the driving current 10 µA, when V_+ and I_+ share the same contact, and V_- and I_- share the same contact. I is calculated as the peak-to-peak voltage, 1 V, of the driving signal divided by the shunt resistance, 100 kΩ, neglecting the voltage dropped by the sample. In order to test the error in the resistance measurements, the two-contact resistance was measured for all adjacent pairs of electrodes. This also helped to verify that the measurements were calibrated properly by comparing the resistances measured to the simulations in LTSpice for the resistor grid [21]. By taking repeat measurements, over a series of scans, the error calculated from the standard deviation was found to be less than 1%.

To summarise, measurements were taken using a driving frequency of 8 kHz, time constant of 1 ms, and a delay time of 20 ms.

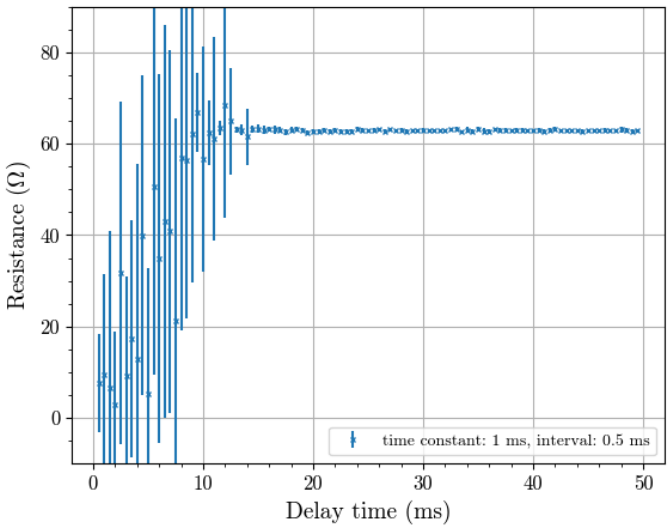

Figure 5: Plot of two-contact resistance measurement as a function of delay time. The time constant used by the lock-in amplifier was 1 ms. Error bars show the standard deviation of ten repeats. Stable measurement occurs by 20 ms.

4.3.2 EIT

In order to assess the adaptive ESA, a series of EIT scans using traditional ESAs, as described in Section 3.2.1, were carried out using the measurement protocol described in Section 4.3.1. The GREIT algorithm was used to reconstruct the conductivity maps using the parameters shown in Table 1. The adjacent-adjacent and opposite-adjacent methods were used. The results are shown in Section 5.1.

The adaptive ESA as described in Section 3.2.2 was also tested using the same protocols and GREIT parameters as for the traditional ESAs. The adaptive

Parameter	Value
λ	0.1
p	0.5
w	1
s	0.2

Table 1: Table of GREIT parameters used. λ is the regularisation parameter; p is the estimated noise covariance; w is the uniform weighting magnitude; and s is the width of the sigmoid function used in the blurring matrix in units of the width of the model.

ESA was implemented such that an initial set of measurements were taken using a traditional ESA, such as the adjacent-adjacent method. From these measurements, a set of current pairs were suggested. For each current pair, a set of voltage pairs were suggested. The corresponding measurements were then taken before repeating the suggestion process using the newly acquired data. This process was then iterated several times until a final reconstruction was made. The adaptive ESA was run several times on Sample A while using different numbers of suggested current pairs, voltage pairs per current pair, and iterations. It was found that for the 32 electrode setup, 2-3 current pairs per iteration, 20-60 voltage pairs per suggested current pair, and 5-10 iterations worked best on visual inspection of the reconstructions. These settings were then used for Sample B. Examples of these reconstructions are shown in Section 5.2.

5 Results and Discussion

5.1 Traditional ESA

The GREIT conductivity map reconstructions for the traditional ESAs are shown in Figure 6. The colour scale shown represents relative change in conductivity. The units are not displayed as the scaling is dependant on the ratio of the measurement geometry to the FEM geometry [13], and this was not determined during the course of the project. Therefore, the reconstructions should be treated qualitatively. One can also see that the magnitudes vary between each reconstruction. This is partly due to the fact that GREIT is a difference EIT method and is not as well suited to determining absolute conductivity compared to absolute EIT algorithms [22].

In each of the reconstructions, there is a region of low conductivity at the top of each plot which corresponds to the region in the resistor networks where the $300\,\Omega$ were located, as shown in Figure 3. Figures 6c and 6d show the conductivity maps for Sample B. Both show another region of low conductivity as well as a region of high conductivity. These regions can be explained by the regions in Sample B where resistors were removed and where $100\,\Omega$ resistors were replaced by $50\,\Omega$ resistors, respectively. The location of the region of low conductivity appears reasonably accurate, when compared to Figure 3. However, the region of low conductivity is inaccurate for both methods.

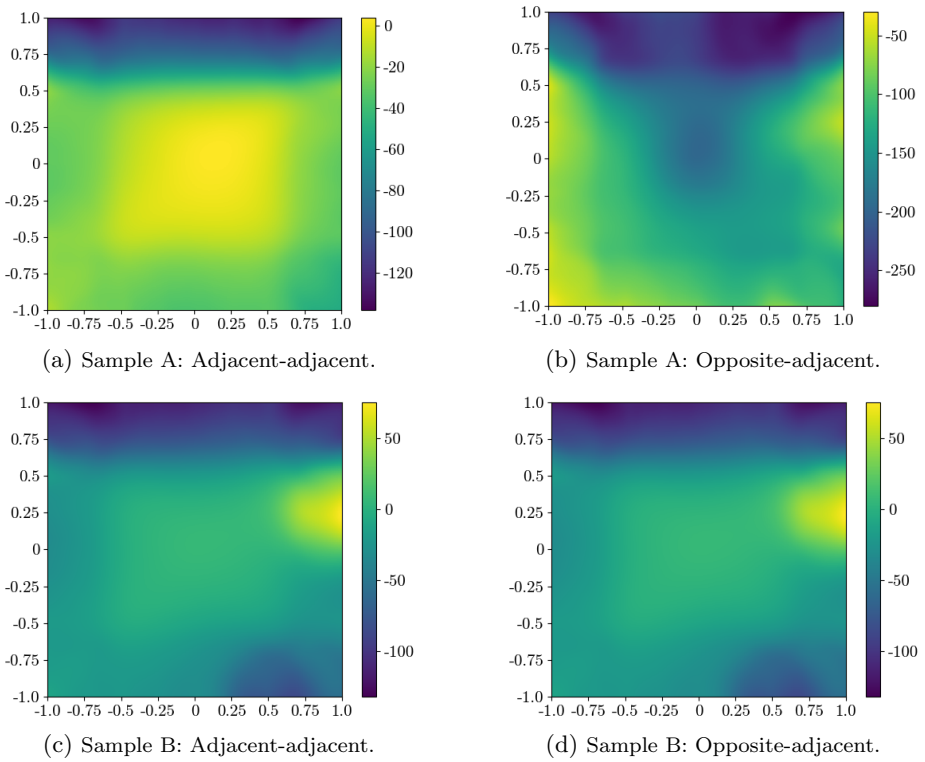

(a) Sample A: Adjacent-adjacent.

(b) Sample A: Opposite-adjacent.

(c) Sample B: Adjacent-adjacent.

(d) Sample B: Opposite-adjacent.

Figure 6: GREIT conductivity reconstructions using the adjacent-adjacent and opposite-adjacent method for two samples(A and B). Colour represents relative change in conductivity compared to an arbitrary reference conductivity.

5.2 Adaptive ESA

The GREIT conductivity map reconstructions for samples A and B using the adaptive ESA are shown in Figure 7. The figure shows how the reconstruction develops as more measurements are added. For both samples, it appears that increasing measurements increases the quality of the reconstruction, as desired. However, this is to be expected for both adaptive and non-adaptive ESAs and on its own is not an indicator of an advantage offered by the adaptive ESA. One can only conclude that the performs better than the traditional ESAs if the reconstruction reaches a comparable quality with fewer measurements. In the reconstructions presented, this seems to be the case as after 553 measurements for Sample A (Figure 7b) and 430 measurements for Sample B (Figure 7b), the reconstructions are comparable to the traditional methods. As the adjacent-adjacent method requires 928 measurements and the opposite-adjacent method requires 896 measurements for 32 electrodes, these initial tests indicate that the adaptive ESA does offer an advantage.

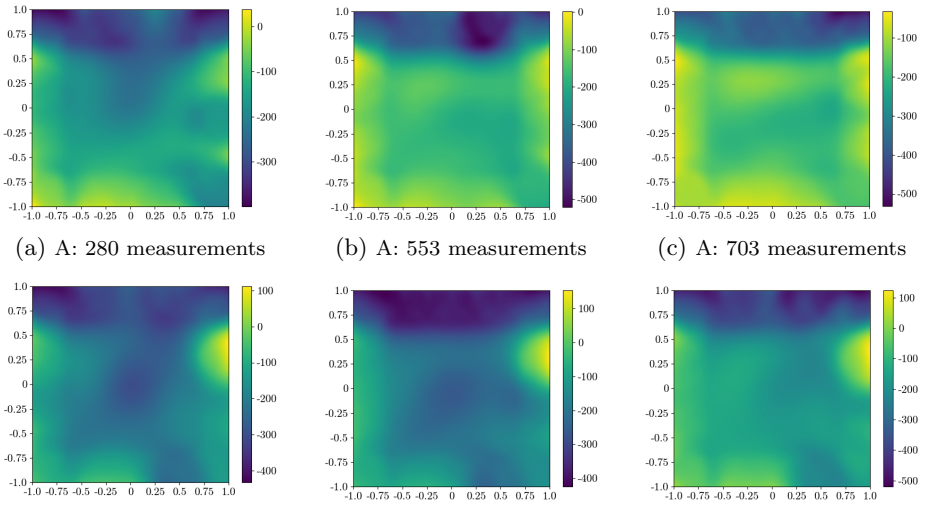

(a) A: 280 measurements (b) A: 553 measurements (c) A: 703 measurements

(d) B: 280 measurements (e) B: 430 measurements (f) B: 732 measurements

Figure 7: GREIT conductivity reconstructions using adaptive ESA for two samples (A and B). Plots show how the reconstructions develop over 1, 5, and 10 iterations of the adaptive ESA. Colour represents relative change in conductivity compared to an arbitrary reference conductivity.

Despite these promising initial results, it will be necessary to quantify this advantage. There is some difficulty in doing so as the error, as defined in Equation 8, cannot be calculate directly as the true target conductivity is unknown. Therefore, it would be challenge to plot, for instance, the loss as a function of time for the adaptive ESA as done in [11] where the target conductivity was a simulated and therefore known. Furthermore, quantifying uncertainty is currently an open problem in EIT [5].

Another limitation of the methodology in this project was the limited sample size. When stating that a machine-learning algorithm is effective, in order to be meaningful it must come with a statement about the training, validation, and test sets [23]. Currently the training data is based on the simulations in [11]. The validation set is used to tune the parameters of the algorithm and in this case was very small, just Sample A. Again, the test set was just a single sample, Sample B. Therefore, a larger number of tests are required and the process of tuning the new parameters (number of current pairs, voltage pairs, and iterations) in the adaptive algorithm should be formalised.

6 Conclusion

In the course of this project a working EIT-system capable of performing conductivity reconstructions using the GREIT algorithm was developed and demonstrated using traditional ESAs. The system was designed for use in solid-state physics with the potential for low signal-to-noise voltage measurements at high speed. Furthermore, the system was capable of performing EIT while using an adaptive ESA with suggestions for current and voltage electrode positions. Initial results are consistent with previous simulations, which indicate that an adaptive ESA enables lower error reconstructions with fewer measurements than traditional ESAs. However, more work must be done in order to verify and quantify this advantage.

References

[1] R. Bayford and R. J. Halter, "Focus on advances in electrical impedance tomography," *Physiol Meas*, vol. 39, no. 9, p. 090301, 09 2018.

[2] A. Cultrera, D. Serazio, A. Zurutuza, A. Centeno, O. Txoperena, D. Etayo, A. Cordon, A. Redo-Sanchez, I. Arnedo, M. Ortolano, and L. Callegaro, "Mapping the conductivity of graphene with Electrical Resistance Tomography," *Sci Rep*, vol. 9, no. 1, p. 10655, Jul 2019.

[3] R. Mann, F. Dickin, M. Wang, T. Dyakowski, R. Williams, R. Edwards, A. Forrest, and P. Holden, "Application of electrical resistance tomography to interrogate mixing processes at plant scale," *Chemical Engineering Science*, vol. 52, no. 13, pp. 2087–2097, Jul. 1997.

[4] K. H. Wei, C. H. Qiu, and K. Primrose, "Super-sensing technology: industrial applications and future challenges of electrical tomography," *Philos Trans A Math Phys Eng Sci*, vol. 374, no. 2070, Jun 2016.

[5] W. R. B. Lionheart, "Eit reconstruction algorithms: pitfalls, challenges and recent developments," *Physiological Measurement*, vol. 25, no. 1, p. 125–142, Feb 2004. [Online]. Available: http://dx.doi.org/10.1088/0967-3334/25/1/021

[6] A. Cultrera and L. Callegaro, "Electrical resistance tomography of conductive thin films," *IEEE Transactions on Instrumentation and Measurement*, vol. 65, no. 9, p. 2101–2107, Sep 2016. [Online]. Available: http://dx.doi.org/10.1109/TIM.2016.2570127

[7] L. Borcea, "Electrical impedance tomography," *Inverse Problems*, vol. 18, no. 6, pp. R99–R136, oct 2002. [Online]. Available: https://doi.org/10.1088/0266-5611/18/6/201

[8] G. Boverman, B. S. Kim, D. Isaacson, and J. C. Newell, "The complete electrode model for imaging and electrode contact compensation in electrical impedance tomography," in *2007 29th Annual International Conference of the IEEE Engineering in Medicine and Biology Society*, 2007, pp. 3462–3465.

[9] "pyeit: A python based framework for electrical impedance tomography," *SoftwareX*, vol. 7, pp. 304 – 308, 2018. [Online]. Available: http://www.sciencedirect.com/science/article/pii/S2352711018301407

[10] P. Hua and E. J. Woo, *Electrical impedance tomography.* Adam Hilger, 1990, ch. Reconstruction Algorithms.

[11] I. Mihov, "EIT simulations: An optimised electrode selection algorithm and sensitivity test of a new forward solver," *4th Year Report, 2nd Sem.*, May 2020. [Online]. Available: https://ufile.io/usclt4nr

[12] S. Martin and C. T. M. Choi, "Nonlinear electrical impedance tomography reconstruction using artificial neural networks and particle swarm optimization," *IEEE Transactions on Magnetics*, vol. 52, no. 3, pp. 1–4, 2016.

[13] A. Adler, J. H. Arnold, R. Bayford, A. Borsic, B. Brown, P. Dixon, T. J. Faes, I. Frerichs, H. Gagnon, Y. G?rber, B. Grychtol, G. Hahn, W. R. Lionheart, A. Malik, R. P. Patterson, J. Stocks, A. Tizzard, N. Weiler, and G. K. Wolf, "GREIT: a unified approach to 2D linear EIT reconstruction of lung images," *Physiol Meas*, vol. 30, no. 6, pp. 35–55, Jun 2009.

[14] A. Adler, J. H. Arnold, R. Bayford, A. Borsic, B. Brown, P. Dixon, T. J. C. Faes, I. Frerichs, H. Gagnon, Y. Gärber, B. Grychtol, G. Hahn, W. R. B. Lionheart, A. Malik, R. P. Patterson, J. Stocks, A. Tizzard, N. Weiler, and G. K. Wolf, "GREIT: a unified approach to 2d linear EIT reconstruction of lung images," *Physiological Measurement*, vol. 30, no. 6, pp. S35–S55, jun 2009. [Online]. Available: https://doi.org/10.1088/0967-3334/30/6/s03

[15] A. Neubauer, "Tikhonov regularisation for non-linear ill-posed problems: optimal convergence rates and finite-dimensional approximation," *Inverse Problems*, vol. 5, no. 4, pp. 541–557, aug 1989. [Online]. Available: https://doi.org/10.1088/0266-5611/5/4/008

[16] A. Adler, P. O. Gaggero, and Y. Maimaitijiang, "Adjacent stimulation and measurement patterns considered harmful," *Physiol Meas*, vol. 32, no. 7, pp. 731–744, Jul 2011.

[17] T. Bronger and G. Thalhammer, "PyVISA," 2020. [Online]. Available: https://github.com/pyvisa

[18] Preferred Networks Inc., "CuPy," 2020. [Online]. Available: https://cupy.dev

[19] G. Jo, M. Choe, S. Lee, W. Park, Y. H. Kahng, and T. Lee, "The application of graphene as electrodes in electrical and optical devices," *Nanotechnology*, vol. 23, no. 11, p. 112001, feb 2012. [Online]. Available: https://doi.org/10.1088/0957-4484/23/11/112001

[20] M. B. Heaney, *Electrical Measurement, Signal Processing, and Displays*. CRC Press, 2003, ch. Electrical Conductivity and Resistivity.

[21] Linear Technology, "Ltspice," 2020. [Online]. Available: https://www.analog.com/en/design-center/design-tools-and-calculators/ltspice-simulator.html

[22] T. de Castro Martins, A. K. Sato, F. S. de Moura, E. D. L. B. de Camargo, O. L. Silva, T. B. R. Santos, Z. Zhao, K. M?eller, M. B. P. Amato, J. L. Mueller, R. G. Lima, and M. de Sales Guerra Tsuzuki, "A Review of Electrical Impedance Tomography in Lung Applications: Theory and Algorithms for Absolute Images," *Annu Rev Control*, vol. 48, pp. 442–471, 2019.

[23] Y. Xu and R. Goodacre, "On Splitting Training and Validation Set: A Comparative Study of Cross-Validation, Bootstrap and Systematic Sampling for Estimating the Generalization Performance of Supervised Learning," *J Anal Test*, vol. 2, no. 3, pp. 249–262, 2018.